Numerical Simulation on Interface Dynamic of Core Coalescence in Double-emulsion Droplet

Hongshi Su[1,2], Zhibin Wang[1,2]*, Ying Chen[1,2], Songping Mo[1,2], Liang An[3]

[1] School of Material and Energy, Guangdong University of Technology, Guangzhou 510006, China

[2] Guangdong Provincial Key Laboratory of Functional Soft Matter, Guangzhou 510006, China

[3] Department of Mechanical Engineering, The Hong Kong Polytechnic University, Hung Hom, Kowloon, China

*Corresponding author:

*Tel.: 0086-20-39322581; fax: 0086-20-39322570; e-mail: wangzhibin@gdut.edu.cn (Zhibin Wang).

Abstract

Double-emulsion droplets are usually taken as reactors in microfluidics for various applications, such as life science, material synthesis and so on, in which a good understanding of the interface behavior of core coalescence is essential but far from be well understand nowadays. In this work, the interface dynamic behavior induced by the core coalescence of a W/O/W double-emulsion droplet is numerically investigated.

Particularly attention is focused on the effects of droplet diameter and the physical properties of the middle phase because of their key roles. The obtained results indicate that the inner interface deformation of core coalescence results in the outer interface deformation and the degree is determined by the middle phase resistance. The inner and outer interfaces both suffer a typical decaying oscillation process but the outer interface suffers smaller. With increasing the viscosity and density of the middle phase, the inner interface deformation coefficient gradually decreases. Whereas for the outer interface

deformation coefficient, it first presents the opposite variation trend; then, the combined effect of the driven force from the inner droplet and the kinetic energy release of the middle phase results in the slight increase of the outer interface deformation coefficient. At last, the expression of the outer interface-deformation is obtained. The results of this work will guide the applications involving the core coalescence in the double-emulsion droplet.

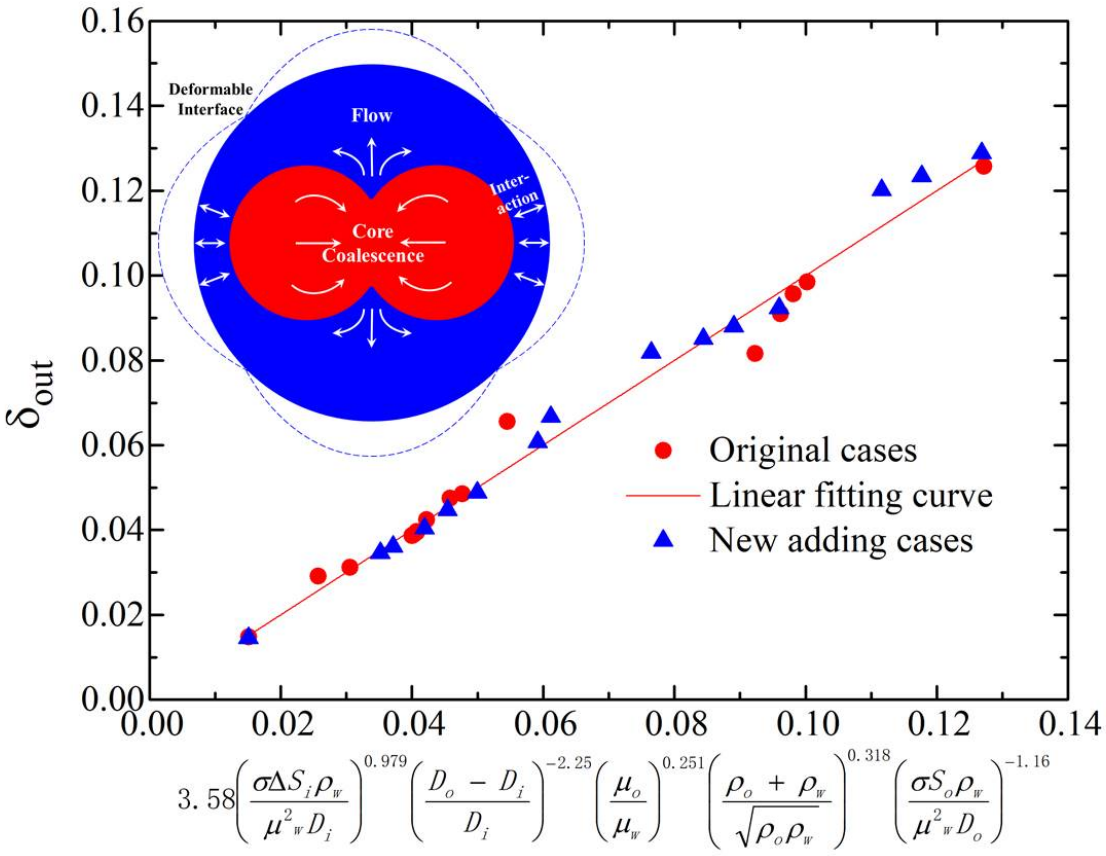

1. Introduction

During the past tens of years, microfluidic chips, be famous as lab-on-a-chip, have been through rapid development and received numerous attention from global researchers due to its intrinsic features such as accuracy, fastness, compact size, low sample consumption, high specific surface area, etc. Among various types of microfluidic devices and systems,

the droplet-based microfluidic chip is one of the most frequently employed and critical configurations. In a typical droplet-based microfluidic chip, every individual droplet serves as an isolated reactor unit, where cross-contamination can be eliminated by the separation between the continuous and dispersed phases. Moreover, the excellent repeatability and accurate flow control have made the droplet-based microfluidic chips the ideal tool for a time-resolved study of transient biological/chemical processes. Based on these fascinating traits, droplet-based microfluidic chips are frequently employed in industrial/researching applications from controlled crystallization [1, 2], sample screening [3, 4] to nanomaterial preparation [5, 6], etc.

In droplet-based microfluidic chips, reaction and product characterization inside a single droplet are often required for sample preparation. To this end, double-emulsion droplets are employed to encapsulate two or more smaller droplets i.e. cores containing different precursor samples. In double-emulsion droplets, the mixing of reactant and the triggering of reaction can be accomplished by the core coalescence. And the reaction process and the product are perpetually restrained within a single droplet. These attractive features are highly favorable for multi-step reaction design and product separation/screening. Such as Hou et al. [7] designed a droplet-based microfluidic chip for micro reaction to detecting glucose in a continuous-flow manner. In their design, double-emulsion droplets were used to finish encapsulating glucose solution and glucose oxidase using two cores, respectively; the subsequent enzyme-catalyzed reaction was triggered by core coalescence. Jia et al [8] utilized the on-demand core coalescence inside a water-in-oil-water (W/O/W) to finish a two-step micro reaction. Guan et al. [9] used the

coalescence between the two inner droplets inside the double-emulsion droplet to trigger the reaction for the synthesis of calcium carbonate particles. They found that the interface dynamic has a major impact on the reaction. During the core coalescence, the rapid release of the surface energy will instantaneously and significantly induce the inner flow and interface deformation, resulting in the strengthening of mass transfer, and have a major impact on the subsequent sample mixing, reaction and droplet stability.

In the presented works of interface dynamics mechanism exploring, most of the attention was focused on the interface behaviors induced by carrying flow, such as break-up [10, 11], hydrodynamics [12], deformation dynamics [13-15] of a double-emulsion droplet in shear flow. However, the investigation of interfacial behaviors induced by coalescence between two inner droplets inside the double-emulsion droplet is rather scarce. The inner interface is firstly reconstructed because of core coalescence and affects the outer interface behavior through the middle phase. Conversely, the outer interface behavior has a major main impact on the inner interface behavior. The complex simultaneous outer-inner interfacial dynamics is not only affected by core composition but also significantly affected by configuration and the spatial confinement of the double-emulsion droplet. The complexity of interface behavior induced by core coalescence makes the underlying mechanism still unclear, which hinders the further application of droplet-based microfluidics.

These complex interfacial behaviors are coupled with the multiphase flow and bio/chemical reaction, which is extremely difficult for direct observation and measurement to acquire local/distributed information of the key physical parameters. Fortunately, with

the fast development of numerical calculation and computer science, many methods have been developed to study interfacial behavior and multiphase flows [16-18]. For example, Level-Set (LS) model [19], Volume-of-Fluid (VOF) model [20], Coupled Level-Set and Volume-of-fluid (CLSVOF) model [21], phase-field model [22], multiphase Lattice Boltzmann method [23], etc. In microscale, VOF and LS models are favorable of interface tracking in multiphase flow and also well balanced in computational cost. However, the volume fraction of the VOF model is a step function when calculating phase distribution and tracking interface, which makes the accurate curvature calculation difficult and the physical properties at the interface unsmoothed; On the other hand, the LS model can't fit the mass conservation, which may induce unauthentic physics during the simulation. CLSVOF method, however, incorporates the merits of LS and VOF and overcomes the drawbacks of both, which has been proven to have great potential in simulating two-phase flow and performing accurate interface tracking [24-28]. In this paper, the dynamic interface behavior, induced by core coalescence of the W/O/W double-emulsion droplet, is simulated using the CLSVOF method and the interfacial tension force is calculated by the continuous surface tension model (CFS). Particular attention is focused on the coupled interfacial behaviors of outer and inner interfaces of the emulsion droplets, as well as the channel wall confinement. The effects of droplet diameter as well as the physical properties of oil including viscosity and density are investigated. The results illustrated that the core coalescence in the double-emulsion leads to the deformation of inner and outer interfaces, and the degree of the outer interface deformation exhibits direct dependence over the size of the double-emulsion droplet and the viscosity and density of

the oil. Moreover, the relationship of outer interface deformation and key physical parameters is obtained based on the dimensionless analysis. The relationship built in this work and the obtained results can be applied in future droplet-based microfluidic device development.

2 Model and method

2.1 Physical and numerical model

In this work, the core coalescence in the W/O/W double-emulsion droplet is numerically studied, and the physical model is illustrated in Fig.1(a) The working fluids used in this paper are oil and water. The double-emulsion droplet (diameter: *D*) is located on the horizontal axis of a circular microchannel. Two inner droplets (diameter: *d*) are placed in its central line. The Bond numbers (the ratio between the gravity force and interfacial tension force) of the inner droplet and outer droplet are 0.001 and 0.007, respectively. The pretty small of Bond numbers makes that the gravity can be ignored. Due to the nature of its axial symmetry, the present model can be simplified into a two-dimension model with the axial symmetry for reducing the computational cost. The calculation region of the simplified model is shown in Fig. 1(b). materials and physical properties are shown in Table 1.

2.2 CLSVOF method and governing equation

The basic idea of the CLSVOF method is that the interface normal curvature is calculated through a smooth LS function, the physical properties are obtained through a smooth Heaviside function, and the interface is adjusted through a conservative VOF

function. In the calculation region, the phase ratio in each control volume is defined by the fluid volume ratio function, α. The method combining with the interface reconstruction method simulates two-phase flow by solving the respective momentum equations and processing the volume ratio of each fluid passing through the region.

The fluid volume ratio function in two-phase flow is defined as below.

$$\alpha = \begin{cases} 0, & oil\ zone \\ 0 \sim 1, & oil - water\ interface. \\ 1, & water\ zone \end{cases} \quad (1)$$

The mass conservation equation can be presented in the following form.

$$\frac{\partial \alpha}{\partial t} + \boldsymbol{v} \cdot \nabla \alpha = 0. \quad (2)$$

In the LS method, the interface is defined through a smooth LS function φ. However, since the signed point in the LS function remains a little distance from the interface, we need to redefine the function of φ based on the function of $\boldsymbol{d}$, which represented the shortest distance from a certain point to the interface. The detailed expression is shown below.

$$\varphi = \begin{cases} -|d|, & In\ the\ water\ phase \\ 0, & At\ the\ interface \\ +|d|, & In\ the\ oil\ phase \end{cases} . \quad (3)$$

For each time step, the LS function should be reinitialized in this model. Then the interface is determined based on solving the mass conservation equation of the LS function.

$$\frac{\partial \varphi}{\partial t} + \boldsymbol{v} \cdot \nabla \varphi = 0. \quad (4)$$

In this method, oil and water are both incompressible Newtonian fluids in the isothermal process. For the dynamics of droplet coalescence, the governing equations include the mass conservation equation also named the continuity equation, and the

momentum equation also named the Navier-Stokes equation. The Euler forms of these equations are shown as follows.

Continuity equation:

$$\frac{\partial \rho}{\partial t} + \mathbf{v} \cdot \nabla \rho = 0. \tag{5}$$

Momentum equation:

$$\frac{\partial (\rho \mathbf{v})}{\partial t} + \nabla \cdot (\mathbf{v}\mathbf{v}\rho) = -\nabla p + \nabla [\mu (\nabla \mathbf{v} + \nabla \mathbf{v}^T)] + \boldsymbol{f_{SV}}. \tag{6}$$

In the above formula, $\mathbf{v}$ is the velocity of the fluid (m/s), ρ is the density (kg/m^3), P is the static pressure (Pa), μ is the dynamic viscosity (Pa·s), T is the symbol of transposition. $\boldsymbol{f_{SV}}$ is the interfacial tension force (N), and it is calculated by a continuous surface tension model (CSF) with the following expression.

$$\boldsymbol{f_{SV}} = \sigma \kappa \boldsymbol{n} \delta_s. \tag{7}$$

In the above formula, $\boldsymbol{n}$ is the unit normal vector in the oil-water interface, κ is the interfacial curvature and δ_s is Delta function of the interface. And the unit normal vector and interfacial curvature can be calculated as shown in Eqs. 8 and 9.

$$\boldsymbol{n} = \frac{\nabla \varphi}{|\nabla \varphi|}|_{\varphi=0}. \tag{8}$$

$$\kappa = \nabla \boldsymbol{n} = \nabla \frac{\nabla \varphi}{|\nabla \varphi|}|_{\varphi=0}. \tag{9}$$

The process of reconstructing the interface requires an evaluation of the VOF flux of each cell mesh containing in the interface. In this study, the PLIC scheme is used for interface reconstruction. In order to smooth the physical properties of the discontinued interface, a smooth Heaviside function $H(\varphi)$ is introduced and defined as below.

$$H(\varphi) = \begin{cases} 1, & \varphi > \epsilon \\ \frac{1}{2}\left[1 + \frac{\phi}{\varepsilon} + \frac{1}{\pi} sin\left(\frac{\pi \phi}{\varepsilon}\right)\right], & |\varphi| \le \epsilon. \\ 0, & \varphi < -\epsilon \end{cases} \tag{10}$$

In the above formula, ε is the numerical thickness of the interface and the value is 1.5l (l is the size of a single mesh). In the computational domain, each control volume will be assigned the appropriate attributes and variables according to the smoothing function $H(\varphi)$. The density ρ and viscosity μ of each control volume are determined according to the following two equations.

$$\rho(\varphi) = \rho_w[1 - H(\varphi)] + \rho_o H(\varphi). \quad (11)$$

$$\mu(\varphi) = \mu_w[1 - H(\varphi)] + \mu_o H(\varphi). \quad (12)$$

In the above formula, "w" and "o" respectively represent the water phase and the oil phase.

2.3 Boundary conditions and numerical solution method

As shown in Fig. 1, the inlet and outlet with the same pressure value are utilized in the model. The wall boundary is the non-slip wall condition. An incompressible flow with low velocity and a Pressure-based solution separation method in Fluent are chosen in the model. PISO is adopted in this study. The high-order QUICK format is used to solve the physical quantity and its derivative of each control volume could be contained in the interface.

The choice of relaxation factor and time step will also have an impact on the convergence and stability of the calculation. Through the analysis of the residual curve and the result, the time step is selected as 10^{-7} and the Courant number C_r number is less than 0.2. The calculation has good stability and convergence. In addition, to ensure the calculation accuracy, the convergence residuals of pressure, density, velocity, and temperature are all set as 10^{-4}.

2.4 Mesh independence verification

The CFD pre-processing software GAMBIT is used for geometric model building and meshing. The regular square mesh is adopted and the mesh is refined in the region of double-emulsion droplet for all cases, as shown in Fig. 1.

The mesh independence test uses five meshes with different mesh numbers. The diameter of the inner droplet is 150 μm and the diameter of the outer droplet is 400 μm. We use hexadecane as the oil phase, and the density and viscosity of oil are 773.4 kg/m^3 and 0.00295 Pa·s, respectively. And the interfacial tension coefficient between the oil and water phase is 0.0432 N/m [29]. The change of dimensionless liquid bridge R(t)/R with time formed by core coalescence is shown in Fig. 2., and the deviation of $R(t)/R$ is calculated and displayed in Table 2. It can be seen that a mesh with mesh numbers 234,000 is sufficiently accurate for this model and will be used for all the below calculations.

2.5 Model verification

To verify the reasonability of the numerical model used in this paper, cases about the partial coalescence between a droplet and a liquid-liquid interface are simulated by using the above-mentioned solution. Then the simulation result is compared with the experimental work of Chen et al. [30] and the numerical results of Ray et al. [31]. The working fluids and their physical properties are the same as the previous works. The comparison result is illustrated in Fig. 3. As shown, the present numerical results show very good agreement with both results of Chen et al. [30] and Ray et al. [31]. Therefore, the numerical model of this paper can be considered to be reasonable.

3 Results and discussion

3.1 Dynamic interface behavior

In this section, the diameters of inner droplets and outer droplet are 150 μm and 400 μm, respectively. We use hexadecane as the oil phase. The development of pressure fields during the coalescence of the inner droplets is illustrated in Fig. 4. At t = 0.023 ms, the two inner droplets are in contact, forming a liquid bridge with a concave interface in the contacting domain. In the meanwhile, a low-pressure region is formed in the aqueous phase of the inner droplet near the concave interface, and the pressure in the other regions remains almost unchanged. This is because the formation of the liquid bridge dramatically changes the local interface curvature. As defined in Eq. (7), the change of the interface curvature and normal vector leads to the change of local surface tension force. Therefore a capillary pressure is rose at the interface decreasing the local water pressure and increasing the oil pressure, which shows excellent agreement with the Young-Laplace equation. In such a case, the driving force from pressure difference leads to water in inner droplets flow from high-pressure region to low-pressure region, that is, the water is continuously transported from other regions to the contact region of inner droplets, which results in the growth of the liquid bridge. As the process continues, at t = 0.11 ms, the liquid-bridge height along the Y-axis reaches its maximum, approaching 67.1 μm. When the height of the liquid bridge is equal to both sides of the inner liquid-liquid interface, we consider that the liquid bridge has been reaching its maximum. And then we stop calculating the liquid bridge. At this time, the water continues to flow from the region away from the liquid bridge into the liquid-bridge region because the pressure in the

liquid-bridge region is still lower than that in the region away from the liquid bridge. During this process, the interface area of the inner droplet gradually decreases accompanying the energy conversion from interface energy to kinetic energy and viscous dissipation until the interface area reaches the minimum (t = 0.25 ms). To more clearly describe the oscillation process, the length of the inner droplet interface at the X-axis direction is extracted, and the result is shown in Fig. 5 (a). It can be found that the amplitude of the inner droplet length at the X-axis direction firstly decreases little and then increases after then it begins to oscillate. This is because the droplets' coalescence is driven by the separation-driven droplet coalescence mechanism [32], in which the droplets are in close with each other, then separates, and moves closer again so that the coalescence happens. After the two droplets contact each other, the inner droplet interface first retracts at the X-axis direction until the length at the X-axis direction reaches its minimum 123.3 μm at 0.28 ms. Subsequently, the length of the inner interface at the X-axis rapidly increases and reaches a maximum at 0.52 ms. After that, the inner droplet exhibits periodic oscillations in which the amplitude is smaller and smaller due to viscous dissipation. Eventually, the oscillation amplitude tends to zero at 2.0 ms, indicating the formation of a stable internal droplet after the coalescence.

Besides, we also analyze the dynamic behavior of the outer interface. The variations with the time on the lengths of the outer interface at the X-axis and Y-axis are illustrated in Fig. 5 (b). As can be found, the two curves show the opposite trend with the opposite peaks, different amplitudes, but the same oscillation periods. The oscillation of the outer interface is induced by the oscillation of the inner interface. For example, the minimum

length, 384.5 μm, of the outer interface at the X-axis is obtained at 0.29 ms. Subsequently, the maximum length, 409.0 μm, of the outer interface at the X-axis is obtained at 0.94 ms. Then it also enters a typical decaying oscillation process. But the amplitude of the outer interface is smaller than the inner interface. Simultaneously, the inner and outer interfaces produce periodic deformation during the inner droplets' coalescence, and the interface deformation gradually decreases until the inner droplet is kept at a stable state.

To characterize the inner and outer interfacial deformation, the interface deformation coefficient δ_{in} and δ_{out} are defined in this paper. The expressions are as follows:

$$\delta_{in} = \frac{D_t - D_{in-min}}{D_t}, \tag{13}$$

$$\delta_{\mathrm{out}} = \frac{D_o - D_{out-min}}{D_o}. \tag{14}$$

The above equations represent the deformation amount of inner and outer interfaces along the X-axis, respectively. In the above formula, D_{in-min} and $D_{out-min}$ represent the minimum values of the length of the inner interface and outer interface at X-axis during the whole process. D_t represents the diameter of the coalesced inner droplet at a stable state and D_o is the initial diameter of the outer droplet. In this case, the values of δ_{in} and δ_{out} are calculated as 0.3 and 0.039, respectively. These results mean that the deformation of the outer interface is quite small than the inner interface.

In the process of the inner droplet coalescing, it is the conversion of the interface energy and the kinetic energy plus the viscous dissipation. The velocities of the inner phase and middle phase and the deformation resistance force have a significant change in this process. To reveal the interaction between inner and outer droplet interfaces, the maximum average velocity of the inner droplet, V_{max-in}, the maximum average velocity

of the middle phase, $V_{max-mid}$, and the deformation resistance force of inner droplet F_m are introduced. The maximum average velocity is extracted from the first oscillation period. The deformation resistance force of the inner droplet is also calculated from the above period. The formula for calculating the deformation resistance force of inner droplet F_m [33] is shown below.

$$F_m = 3\pi D\mu_o V_{max-in} \frac{1+2\mu_o/3\mu_i}{1+\mu_o/\mu_i}. \quad (15)$$

In this formula, D is the inner droplet diameter, μ_o is the middle-phase viscosity, μ_i is the viscosity of the inner droplet.

In this case, the maximum average velocity values of inner droplet V_{max-in} and the middle phase $V_{max-mid}$ are 0.742 m/s and 0.0683 m/s, respectively. The deformation resistance force of the inner droplet is calculated as 2.93 μN. It can be seen that the viscous dissipation is the main loss of the kinetic energy between inner and outer interfaces. The calculation results of each physical parameter, in this case, are summarized in Table 3.

3.2 Effect of inner droplets' diameters

In the previous section, we have found that the coalescence of inner droplets can induce the deformation of the outer interface. And the diameter of the inner droplet has a major impact on the dynamic behavior of the inner and outer interface. Thus the impact of the inner droplet diameter on the interface behaviors is discussed in this section. The diameter of the outer droplet is kept at 400 μm. And the oil phase is still hexadecane. To describe the relative size between the inner droplet and out droplet, the inner-outer droplet diameter ratio $k = D_i/D_o$ is introduced, where D_i and D_o are the diameters of the inner

droplet and outer droplet, respectively.

The variations about *R(t)/R* with time under different droplet diameters are illustrated in Fig. 6. As shown, the growth rate of *R(t)/R* is higher for smaller inner droplets. For example, *R(t)/R* reaches 0.89 at 0.0636 ms when the diameter of inner droplets is 120 μm; while it reaches the same value at 0.1198 ms for the inner droplets' diameter of 190 μm. This is because the fluid to be driven is more and the velocity is lower when the diameter is larger. Figure 7 (a) shows the interface behavior with the increase of the diameter ratio, *k*, the inner interface deformation coefficient δ_{in} is firstly increased from 0.296 to 0.3 and then decreased from 0.3 to 0.279, while the outer interface deformation coefficient δ_{out} is persistently increased from 0.0148 to 0.1258. This is because more interface energy of the previous inner droplets is converted to the kinetic energy of the coalesced droplet. And the deformation of the coalesced droplet drives the movement of the middle phase, which induces the deformation of the outer interface. Due to constant outer diameter, the middle phase becomes less for larger inner droplets, and the constraint from the outer interface to coalesced droplet becomes stronger for larger inner droplets. As a result, the inner interface deformation coefficient δ_{in} firstly increases and then decreases, while the outer interface deformation coefficient δ_{out} is increased by increasing the inner size. The reason for these phenomena can be confirmed by the deformation resistance force of the inner droplet and velocities of the inner droplet and middle phase shown in Fig. 7 (b). The deformation resistance force of the inner droplet is increased from 2.5 μN to 3.63 μN and the maximum velocity of the inner droplet is reduced and the middle phase maximum velocity is increased with increasing the inner droplet diameter. When the inner

droplet diameter is smaller than 150 μm, the inner-outer droplet diameter ratio is smaller. The movement of the inner interface is smaller limited by the outer interface comparing with the basic case. So the constraint from the middle phase on the inner droplet is weak. Meanwhile, when the diameter of the inner droplet is more than 150 μm, the inner-outer droplet diameter ratio is larger. The movement of the inner interface is larger limited by the outer interface comparing with the basic case. So the constraint from the middle phase on the inner droplet becomes stronger. Thus, the inner interface deformation coefficient δ_{in} gradually decreases. For the outer interface, the interaction from the inner interface through the middle phase is strengthened. And the constraint from the continuous phase is unchanged. As a result, the outer interface deformation coefficient δ_{out} is increased.

3.3 Effect of the double-emulsion droplet's diameters with a fixed inner-outer diameter ratio

In this section, the impact of the double-emulsion droplet's diameter with a fixed inner-outer diameter ratio will be discussed. Diameters of the outer droplet and inner droplet are increased from 320 μm to 500 μm and 144 μm to 225 μm, respectively. The oil phase is still hexadecane.

The variations about *R(t)/R* with time for different diameters of the double-emulsion droplet are illustrated in Fig. 8. It can be seen that the growth rate of *R(t)/R* is increased by increasing the diameter of the double-emulsion droplet. As shown, *R(t)/R* reaches 0.89 at 0.0822 ms when the double-emulsion-droplet diameter is 144/320 μm, whereas it gradually increases to 0.1517 ms when the diameter is 225/500 μm. It is easy to understand that the same bridge height for smaller inner droplets can play a more

significant role. The variation trends of δ_{in} and δ_{out} are shown in Fig. 9 (a). As shown, when the double-emulsion-droplet diameter is increased from 144/320 μm to 225/500 μm, the values of δ_{in} and δ_{out} are gradually increased from 0.284 to 0.297 and decreased from 0.098 to 0.082, respectively. Such opposite variation trend for δ_{in} and δ_{out} could be ascribed to the disparity of the middle phase. With increasing the double-emulsion-droplet diameter, the constraint from the outer interface on the inner droplet is weakened, leading to the inner interface deformation coefficient δ_{in} gradually increase. It can be confirmed from the deformation resistance force of the inner droplet, the maximum velocity of the inner droplet and middle phase, which are all are decreased and shown in Fig. 9 (b). For example, the deformation resistance force of the inner droplet decreases from 4.24 μN to 2.59 μN when the diameter of the double-emulsion droplet is increased from 144/320 μm to 225/500 μm. As for the outer interface, the interaction from the inner interface on the middle phase becomes weaker when the double-emulsion-droplet diameter is increased. Moreover, the constraint from the continuous phase on the middle phase is unchanged. As a result, the outer interface deformation coefficient gradually decreases. In summary, the inner interface deformation coefficient δ_{in} is increased as increasing the double-emulsion-droplet diameter and the outer interface deformation coefficient δ_{out} is reduced.

3.4 Effect of the oil viscosity and density

As found, the oil phase (middle phase) has a major impact on the interaction between the inner and outer interfaces. The viscosity and density are two of the most important physical properties on flow dynamic behavior. In this section, the effects of oil viscosity

and density on the interface behavior are studied. Diameters of the inner droplet and outer droplet are 150 μm and 400 μm, respectively. To do this, the density of oil is kept at 774.3 kg/m^3 for researching the effect of the oil viscosity, and the oil viscosity is kept at 0.00295 Pa·s for study the effect of oil density. The viscosity ratio $\lambda = \mu_o/\mu_w$ and density ratio $\beta=\rho_o/\rho_w$ are introduced to reflect the relative relation of correspondence physical property between oil and water. The interfacial behavior induced by core coalescence is investigated as follows.

The variations about *R(t)/R* with time under different oil viscosity are illustrated in Fig. 10. We can see that the growth rate of *R(t)/R* is decreased with increasing the viscosity ratio. *R(t)/R* reaches the maximum value of 0.897 at 0.0831 ms when the oil viscosity is 0.00050 kg/(m·s). While *R(t)/R* reaches the maximum value of 0.891 at 0.098 ms when the oil viscosity is 0.0100 kg/(m·s). This is because the deformation resistance force of the inner droplet increases when the oil viscosity o increases, resulting in the lower speed of the inner interface deformation. The variation trends of the inner and outer interface deformation coefficients δ_{in} and δ_{out} with λ are shown in Fig. 11 (a). It can be found that the inner interface deformation coefficient δ_{in} is reduced when the viscosity ratio λ is increased. But the variation trend of outer interface deformation coefficient δ_{out} is the opposite. The value of δ_{in} is reduced from 0.370 to 0.207 and the value of δ_{out} is increased from 0.029 to 0.066 when the viscosity ratio is increased from 0.5 to 10. As illustrated in Fig. 11 (b), the deformation resistance force of the inner droplet is increased when the viscosity of oil increases. The deformation of the inner droplet is greatly constrained by the middle phase. As a result, the inner interface deformation coefficient is

reduced. This also can be verified from the maximum velocity of the inner droplet, as illustrated in Fig11 (b). For the outer interface, when the oil viscosity increases, the viscous friction of the middle phase increases, resulting in decreasing the maximum velocity of the middle phase. However, from the aspect of the middle phase, the action from the inner interface on the middle phase becomes stronger. While the constraint from the continuous phase on the middle phase remains unchanged. Therefore the outer interface deformation coefficient is increased with increasing the viscosity of the middle phase of oil.

The variations about *R(t)/R* with time under different oil density are displayed in Fig. 12. As shown, the growth rate of *R(t)/R* is reduced with increasing the density of oil (density ratio β). For example, *R(t)/R* reaches the maximum value 0.895 at 0.0743 ms when the density of oil is 99.82 kg/m^3 (β=0.1), and it reaches the maximum value 0.893 at 0.1015 ms when the density of oil is 1996.4 kg/m^3 (β=2.0). The growth of the water bridge induced by the core coalescence drives the movement of the oil phase. During the inner-interface reconstruction, the more kinetic energy from the inner droplet transfers to the oil phase when the density of oil becomes heavier. Such that the growing rate of the bridge height is lower for a larger value of oil's density.

The variation trends of interface deformation coefficients δ_{in} and δ_{out} with the density ratio β are shown in Fig. 13 (a). As can be seen, the values of δ_{in} is increased from 0.2856 to 0.3094 when β is increased from 0.1 to 2. Whereas for the outer interface deformation coefficient δ_{out}, it is firstly reduced from 0.04847 to 0.03863, and then slightly rises to 0.03943. The inner-droplet deformation drives the middle-phase

movement. The larger density of the middle phase can effectively reduce the velocity of the middle phase and inner droplet, which is shown in Fig. 13(b). Accordingly, the viscous dissipation is minimized, resulting in converting more interface energy to kinetic energy and then further converting to interface energy. The more interface energy means the larger value of the interface deformation coefficient. Therefore the inner interface deformation coefficient δ_{in} is increased with increasing the density of the oil phase. Whereas for the outer interface deformation coefficient δ_{out}, when the density of oil is increased from 0.1 to 1, because of the gradually decreased velocity of the oil, the deformation resistance force of the inner droplet, which is illustrated in Fig. 13(b), is reduced. However, when the oil density further increases, more inner interface energy can be converted to the middle-phase kinetic energy, it can be confirmed by the results of the kinetic energy of the middle phase which is shown in Fig. 13(b). Such higher kinetic energy of the middle phase strengthens the deformation of the outer interface, leading to the outer interface deformation coefficient slightly increases with further increasing the oil density from 1.0 to 2.0.

3.5 The discussion of correlation

Above the discussion, we can find that the deformation of inner and outer interfaces, induced by the core coalescence, is affected by not only the size of the double-emulsion droplet but also the viscosity and density of the middle oil-phase. The inner interface deformation is directly resulted by the core coalescence which is a process of the reconstruction of the inner interface. Then the inner interface deformation is transmitted to the outer interface through the middle-oil-phase shell. In this process, the surface energy

of the inner interface reduces and converts into kinetic energy and viscous dissipation. And then, a part of kinetic energy transmits to the outer interface. In the whole process, the reducing surface energy of the inner interface can be seen as the driving force and the middle-oil-phase shell can be seen as the transmission resistance. Therefore, it can be found that the outer interface deformation is mainly impacted by the driving force and the transmission resistance. The amount of the driving force is mainly controlled by the inner droplet including the size, viscosity, and density. The amount of transmission resistance is mainly determined by the middle-oil-phase, including shell thickness, viscosity, and density. In addition, the outer interface deformation is also affected by itself of the outer interface. Thus, the deformation of the outer interface in all cases can be described as the following equation,

$$\delta_{out} \sim \alpha = A\left(\frac{\sigma \Delta S_i \rho_w}{\mu_w^2 D_i}\right)^a \left(\frac{D_o - D_i}{D_i}\right)^b \left(\frac{\mu_o}{\mu_w}\right)^c \left(\frac{\rho_o + \rho_w}{\sqrt{\rho_o \rho_w}}\right)^d \left(\frac{\sigma S_o \rho_o}{\mu_o^2 D_o}\right)^e \quad (16)$$

In the above equation, the items of the right side from left to right mean the surface energy item, the thickness of the middle-oil-phase shell item, the viscosity item, and the density item. In the surface energy item, $\sigma \Delta S_i$ represents the reducing surface energy of the inner interface after the coalescence of two inner-droplets. And σS_o is the surface energy of the outer interface. To make the surface energy item dimensionless and consider the contribution of the viscosity and density of the inner phase, $\frac{\mu^2 D}{\rho}$ is introduced according to the dimensional analysis. μ, D, ρ represents the viscosity of the oil, the diameter of the droplet, and the density of the oil, respectively. The subscript *i* and *o* represent the inner droplet and the outer droplet, respectively. Then the linear fitting curve is obtained according to the above all cases shown in Fig. 14. The values of *A*, *a*, *b*, *c*, and *d* are 3.58,

0.979, -2.25, 0.251, 0.381and -1.16, respectively. The above equation can be rewritten as the following form according to the linear fitting curve.

$$\delta_{out} = 3.58\left(\frac{\sigma\Delta S_i\rho_w}{\mu^2{}_w D_i}\right)^{0.979}\left(\frac{D_o - D_i}{D_i}\right)^{-2.25}\left(\frac{\mu_o}{\mu_w}\right)^{0.251}\left(\frac{\rho_o + \rho_w}{\sqrt{\rho_o\rho_w}}\right)^{0.318}\left(\frac{\sigma S_o\rho_w}{\mu^2{}_w D_o}\right)^{-1.16} \quad (17)$$

In Fig. 14, the black dots represent cases of section 3.2~3.5, the red line represents the linear fitting curve, and the blue dots are newly added cases. It can be seen that the blue dots distribute along the red line. It has a high degree of coincidence. The maximum error of all dots including black and blue dots is less than 19.2%, and the average error is less than 4.5%. Therefore, the equation is sufficiently reliable to be used to describe the out-interface deformation of the double-emulsion droplet induced by the inner-droplets coalescence.

4 Conclusions

We employ the CLSVOF method to numerically study the core coalescence in the double-emulsion droplet. And the interfacial tension force is simulated through the CSF model. The interface dynamic behavior about the core coalescence in the double-emulsion droplet is analyzed. The results show that inner and outer interfaces both periodically suffer decaying oscillation after the core coalescence with surface energy converting into kinetic energy and viscous dissipation. And the effects of inner droplet diameter, the double-emulsion droplet diameter with the fixed inner/outer diameter ratios, the oil physical properties including density and viscosity are also explored. It is shown that when the inner droplet radius increases, the deformation coefficient of the inner interface induced by the core coalescence increases firstly and then decreases because the constraint

of the outer interface becomes stronger. So the deformation coefficient of the outer interface is increasing. For the fixed inner/outer diameter ratio, the inner interface deformation coefficient is gradually increased as the diameter of the double-emulsion droplet is increased because of the weaker constraint from the outer interface, but the interface deformation coefficient of the outer droplet is gradually decreased due to higher middle phase resistance. With increasing the viscosity of the oil phase, the inner interface deformation coefficient is reduced due to increasing the deformation resistance force, and the outer interface deformation coefficient increases because of the increasing of the driven force. For the effect of the oil density, the inner interface deformation coefficient is increased resulted from the low deformation resistance force and the outer interface deformation coefficient is firstly reduced and then increased when the density of the oil phase is increased because of the combined effect of driven force from the inner droplet and the kinetic energy of the middle phase. Finally, the relationship of the outer interface deformation coefficient is obtained. The results in this paper will guide the applications involving the core coalescence in a double-emulsion.

Acknowledgements

The authors acknowledge the financial supports of the National Natural Science Foundation of China (No. 51806038), Natural Science Foundation of Guangdong Province (No. 2019A1515012119) and Guangdong Special Support Program (2017TX04N371).

References

[1] Zheng, B.; Tice, J. D.; Roach, L. S.; Ismagilov, R. F. A droplet-based, composite pdms/glass capillary microfluidic system for evaluating protein crystallization conditions by microbatch and vapor-diffusion methods with on-chip x-ray diffraction. Angew. Chem.-Int. Edit. **2004**, 43, 2508-2511, DOI: 10.1002/anie.200453974.

[2] Yeap, E. W. Q.; Ng, D. Z. L.; Lai, D.; Ertl, D. J.; Sharpe, S. Continuous Flow Droplet-Based Crystallization Platform for Producing Spherical Drug Microparticles. Org. Process Res. Dev. **2019**, 23, 93-101, DOI: 10.1021/acs.oprd.8b00314.

[3] Li, W.; Zhang, L. Y.; Ge, X. H.; Xu, B. Y.; Zhang, W. X.; Qu, L. L.; Choi, C. H.; Xu, J. H.; Zhang, A.; Lee, H. M.; Weitz, D. A. Microfluidic fabrication of microparticles for biomedical applications. Chem. Soc. Rev. **2018**, 47, 5646-5683, DOI: 10.1039/c7cs00263g.

[4] Payne, E. M.; Holland-Moritz, D. A.; Sun, S. W.; Kennedy, R. T. High-throughput screening by droplet microfluidics: perspective into key challenges and future prospects. Lab Chip **2020**, 20, 2247-2262, DOI: 10.1039/d0lc00347f.

[5] Shum, H. C.; Abate, A. R.; Lee, D.; Studart, A. R.; Wang, B. G.; Chen, C. H.; Thiele, J.; Shah, R. K.; Krummel, A.; Weitz, D. A. Droplet Microfluidics for Fabrication of Non-Spherical Particles. Macromol. Rapid Commun. **2010**, 31, 108-118, DOI: 10.1002/marc.200900590.

[6] Hamdallah, S. I.; Zoqlam, R.; Erfle, P.; Blyth, M.; Alkilany, A. M.; Dietzel, A.; Qi, S. Microfluidics for pharmaceutical nanoparticle fabrication: the truth and the myth. Int. J. Pharm. **2020**, 584, 119408, DOI: 10.1016/j.ijpharm.2020.119408.

[7] Hou, L. K.; Ren, Y. K.; Jia, Y. K.; Deng, X. K.; Liu, W. Y.; Feng, X. S.; Jiang, H. Y. Continuously Electrotriggered Core Coalescence of Double-Emulsion Drops for Microreactions. Appl. Mater. Interfaces **2017**, 9, 12282-12289, DOI: 10.1021/acsami.7b00670.

[8] Jia, Y. K.; Ren, Y. K.; Liu, W. Y.; Hou, L. K.; Tao, Y.; Hu, Q. M.; Jiang, H. Y. Correction: Electro-coalescence of paired droplets encapsulated in double-emulsion drops. Lab Chip **2016**, 16, 4466-4466, DOI: 10.1039/c6lc01052k.

[9] Guan, X. W.; Hou, L. K.; Ren, Y. K.; Deng, X. K.; Lang, Q.; Jia, Y. K.; Hu, Q. M.; Tao, Y.; Liu, J. W.; Jiang, H. Y. A dual-core double emulsion platform for osmolarity-controlled microreactor triggered by coalescence of encapsulated droplets. Biomicrofluidics **2016**, 10, 034111, DOI: 10.1063/1.4952572.

[10] Chen, H. S.; Li, J. A.; Shum, H. C.; Stone, H. A.; Weitz, D. A. Breakup of double emulsions in constrictions. Soft Matter **2011**, 7, 2345-2347, DOI: 10.1039/c0sm01100b

[11] Li, J. A.; Chen, H. S.; Stone, H. A. Breakup of Double Emulsion Droplets in a Tapered Nozzle. Langmuir **2011**, 27, 4324-4327, DOI: 10.1021/la200473h.

[12] Chen, Y. P.; Liu, X. D.; Shi, M. H. Hydrodynamics of double emulsion droplet in shear flow. Appl. Phys. Lett. **2013**, 102, 051609, DOI: 10.1063/1.4789865.

[13] Kim, S.; Dabiri, S. Transient dynamics of eccentric double emulsion droplets in a simple shear flow. Phys.rev.fluids **2017**, 2, 104305, DOI: 10.1103/PhysRevFluids.2.104305.

[14] Zhang, C. B.; Yu, C.; Liu, X. D.; Jin, O.; Chen, Y. P. Steady deformation characteristics of double emulsion droplet in shear flow. Acta Phys. Sin. **2016**, 65, 204704, DOI: 10.7498/aps.65.204704.

[15] Chen, Y. P.; Liu, X. D.; Zhao, Y. J. Deformation dynamics of double emulsion droplet under shear. Appl. Phys. Lett. **2015**, 106, 141601, DOI: 10.1063/1.4916623.

[16] Wang, Z. B.; Chen, R.; Wang, H.; Liao, Q.; Zhu, X.; Li, S. Z. An overview of smoothed particle hydrodynamics for simulating multiphase flow. Appl. Math. Model. **2016**, 40, 9625–9655, DOI: 10.1016/j.apm.2016.06.030.

[17] Nikolopoulos, N.; Nikas, K. S.; Bergeles, G. A numerical investigation of central binary collision of droplets. Comput. Fluids **2009**, 38, 1191-1202, DOI: 10.1016/j.compfluid.2008.11.007.

[18] Li, S. Z.; Chen, R.; Wang, H.; Liao, Q.; Zhu, X.; Wang, Z. B. Simulation on the coalescence of the moving liquid column and droplet in a hydrophilic microchannel by volume of fluid method. Appl. Therm. Eng. **2014**, 64, 129-138, DOI: 10.1016/j.applthermaleng.2013.12.017.

[19] Tatineni, M.; Zhong, X. L. Numerical study of two-phase flows in microchannels using the level set method. AIAA J. **2004**, 0929, Doi:10.2514/6.2004-929.

[20] Brackbill, J. U.; Kothe, D. B.; Zemach, C. A continuum method for modeling surface tension. J. Comput. Phys. **1992**, 100, 335-354, DOI: 10.1016/0021-9991(92)90240-Y.

[21] Sussman, M.; Puckett, E. G. A Coupled Level Set and Volume-of-Fluid Method for Computing 3D and Axisymmetric Incompressible Two-Phase Flows. J. Comput. Phys. **2000**, 162, 301-337, DOI: 10.1006/jcph.2000.6537.

[22] Yu, Z. L.; Qin, T. Y.; Lian, G. P. Numerical simulation of droplet flow in a three dimensional microfluidic devices. Mech. Eng. **2007**, 29, 31-33, DOI: 10.1016/S1874-8651(08)60032-0.

[23] Hou, Y. Z.; Deng, H.; Du, Q.; Jiao, K. Multi-component multi-phase lattice Boltzmann modeling of droplet coalescence in flow channel of fuel cell. J. Power Sources **2018**, 393, 83-91, DOI: 10.1016/j.jpowsour.2018.05.008.

[24] Albadawi, A.; Donoghue, D. B.; Robinson, A. J.; Murray, D. B.; Delaure, Y. M. C. On the analysis of bubble growth and detachment at low Capillary and Bond numbers using Volume of Fluid and Level Set methods. Chem. Eng. Sci. **2013**, 90, 77-91, DOI: 10.1016/j.ces.2012.12.004.

[25] Chakraborty, I.; Biswas, G.; Ghoshdastidar, P. S. Bubble generation in quiescent and co-flowing liquids. Int. J. Heat Mass Transfer **2011**, 54, 4673-4688, DOI: 10.1016/j.ijheatmasstransfer.2011.06.010.

[26] Li, S. Z.; Chen, R.; Wang, H.; Liao, Q.; Zhu, X.; Wang, Z. B.; He, X. F. Numerical investigation of the moving liquid column coalescing with a droplet in triangular microchannels using CLSVOF method. Sci. Bull. **2015**, 60, 1911-1926, DOI: 10.1007/s11434-015-0924-7.

[27] Chen, R.; Li, S. Z.; Wang, H.; Liao, Q.; Zhu, X.; Fan, Q. L.; He, X. F.; Wang, Z. B. Dynamic Behavior of the Liquid Flow Coalescing with a Droplet in Hydrophobic Microchannels. J. Nanosci. Nanotechnol. **2015**, 15, 2923-2931, DOI: 10.1166/jnn.2015.9674.

[28] Wang, Z. B.; Li, S. Z.; Chen, R.; Zhu, X.; Liao, Q.; Ye, D. D.; Zhang, B. Numerical study on dynamic behaviors of the coalescence between the advancing liquid meniscus and multi-droplets in a microchannel using CLSVOF method. Comput. Fluids **2018**, 170, 341-348, DOI: 10.1016/j.compfluid.2018.05.014.

[29] Ndao, M.; Devémy, J.; Ghoufi, A.; Malfreyt, P. Coarse-Graining the Liquid–Liquid Interfaces with the MARTINI Force Field: How Is the Interfacial Tension Reproduced? J. Chem. Theory Comput. **2015**, 11, 3818-3828, DOI: 10.1021/acs.jctc.5b00149.

[30] Chen, X. P.; Mandre, S.; Feng, J. J. Partial coalescence between a drop and a liquid-liquid interface. Phys. Fluids **2006**, 18, 051705, DOI: 10.1063/1.2201470.

[31] Ray, B.; Biswas, G.; Sharma, A. Generation of secondary droplets in coalescence of a drop at a liquid–liquid interface. J. Fluid Mech. **2010**, 655, 72-104, DOI: 10.1017/S0022112010000662.

[32] Chen, H. S.; Zhao, Y. J.; Li, J.; Guo, M.; Wan, J. D.; Weitz, D. A.; Stone, H. A. Reactions in double emulsions by flow-controlled coalescence of encapsulated drops. Lab Chip **2011**, 11, 2312-2315, DOI: 10.1039/c1lc20265k.

[33] White, F. M.; Corfield, I. Viscous fluid flow. McGraw-Hill New York, 2006.

Table list

Table 1 Physical properties of fluids

working fluid	density(kg/m³)	viscosity(Pa·s)	interfacial tension coefficient (N/m)
water	998.2	0.001003	0.0432
oil	99.82~1996.4	0.0005~0.0100	

Table 2 Mesh test

Number of meshes	Calculation time per step	Deviation
37440	4s	<8.6%
58500	4.62s	<3.6%
149760	5.45s	<1.1%
234000	8.57s	<0.3%
351375	15s	/

Table 3 Computational results of different physical parameters

parameter	δ_{in}	δ_{out}	V_{max-in}	$V_{max-mid}$	F_m
value	0.300	0.039	0.742	0.0683	2.93
unit	1	1	m/s	m/s	μN

Figure captions

Figure 1 Physical model (a) and numerical model (b) of core coalescence of a double-emulsion droplet.

Figure 2 Mesh independence test.

Figure 3 Model test. (a) Qualitative comparison of our results with numerical results of Ray et al.[31] and experimental results of Chen et al.[30], and (b) Quantitative comparison of our results with experimental results of Chen et al.[30].

Figure 4 Pressure fields during the core coalescence process.

Figure 5 (a) The distance of inner droplet along the X-axis, and (b) outer droplet along the X-axis and Y-axis.

Figure 6 The variation of the liquid bridge with time under different inner droplets' diameter.

Figure 7 (a) Effect of inner droplets' diameter on the inner and outer interface deformation, and (b) the maximum velocity of the inner droplet and middle phase and the deformation resistance force of inner droplet.

Figure 8 Effect of the double-emulsion droplet's diameters with fixed inner-outer diameter ratio on a liquid bridge.

Figure 9 (a) Effect of the double-emulsion droplet's diameters with fixed inner-outer diameter ratio on the inner and outer interface deformation, and (b) the maximum velocity of the inner droplet and middle phase and the deformation resistance force of inner droplet.

Figure 10 The change of the liquid bridge with time under different oil viscosity.

Figure 11 (a) Effect of the oil viscosity on the inner and outer interface deformation, and (b) the maximum velocity of the inner droplet and middle phase and the deformation resistance force of inner droplet.

Figure 12 The change of the liquid bridge with time under different oil density.

Figure 13 (a) Effect of the oil density on the inner and outer interface deformation, and (b) the maximum velocity of the inner droplet and kinetic energy of the middle phase and the deformation resistance force of inner droplet.

Figure 14 The relationship between different factors and the deformation amount of outer interface.

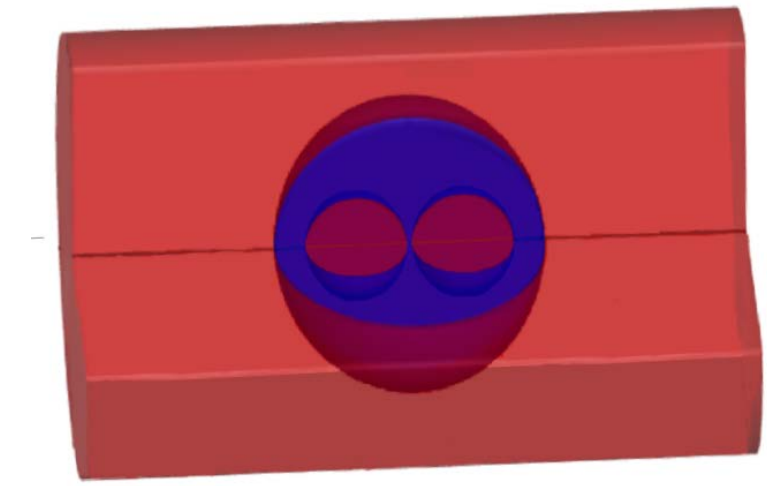

(a)

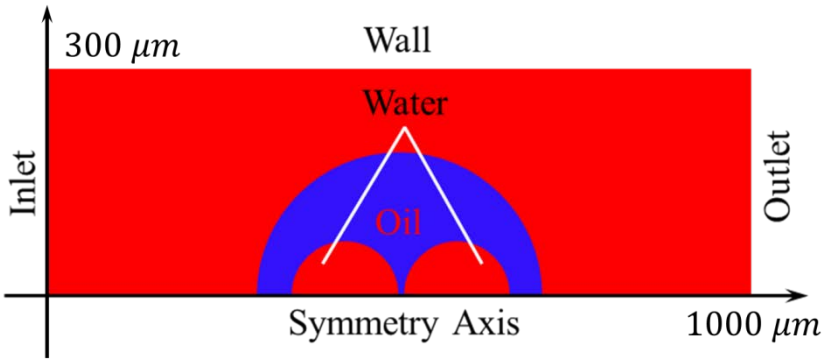

(b)

Fig. 1 Physical model (a) and numerical model (b) of core coalescence of a double-emulsion droplet.

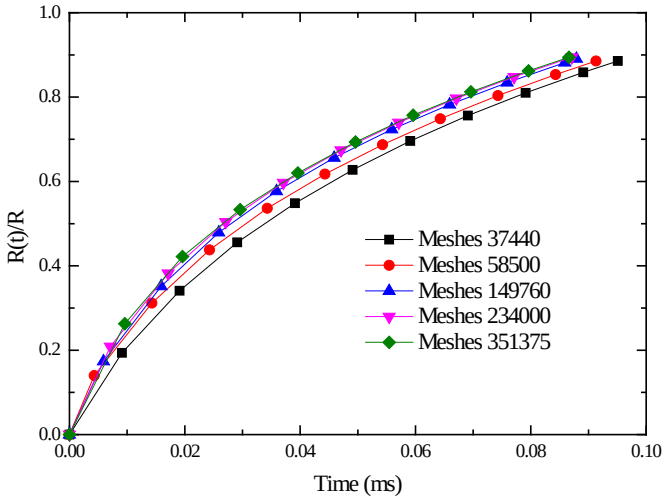

Fig. 2 Mesh independence test.

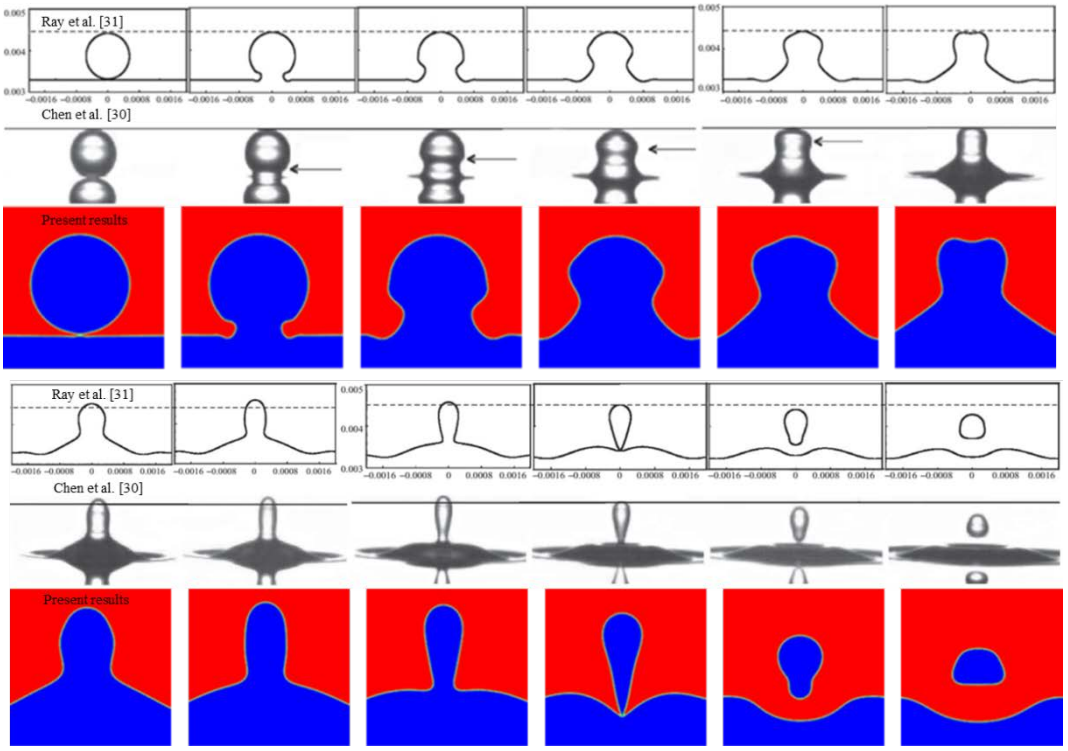

(a)

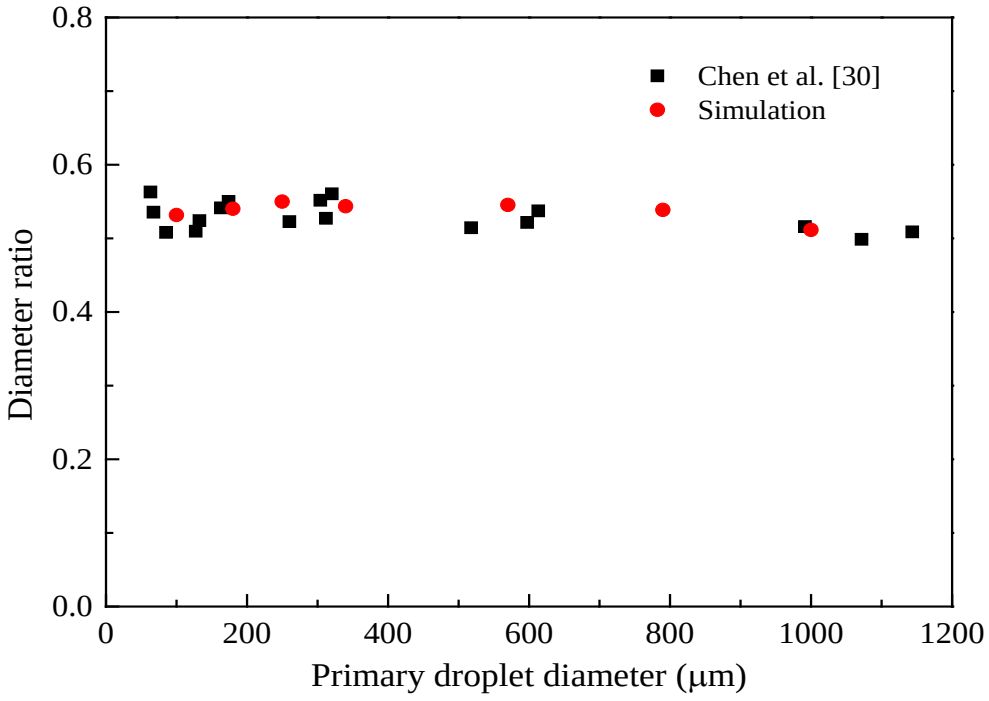

(b)

Fig. 3 Model test. (a) Qualitative comparison of our results with numerical results of Ray et al.[31] and experimental results of Chen et al.[30], and (b) Quantitative comparison of our results with experimental results of Chen et al.[30].

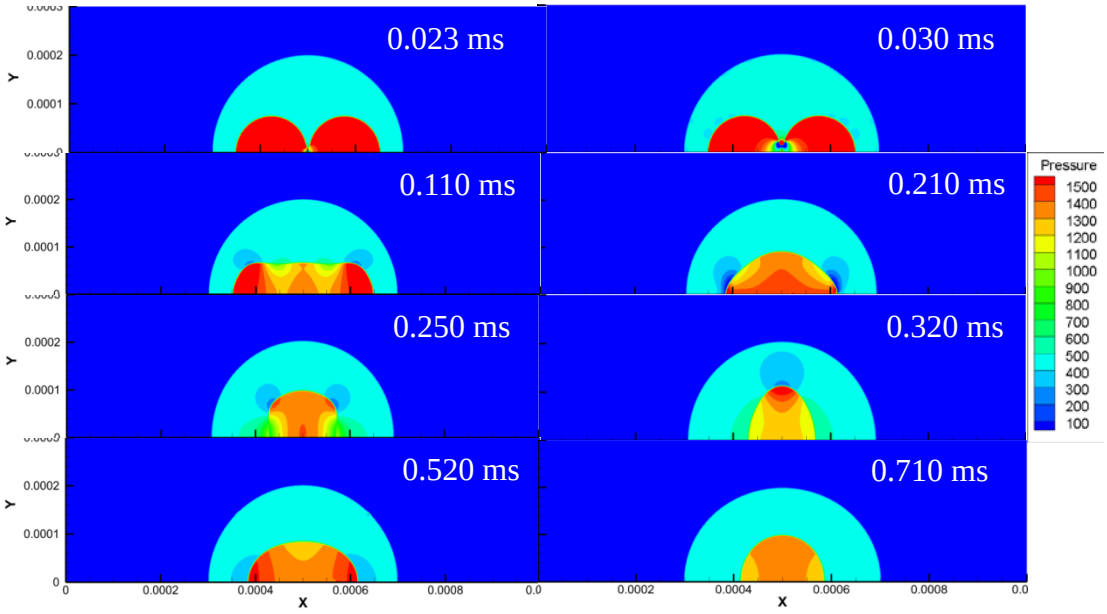

Fig. 4 Pressure fields during the core coalescence process.

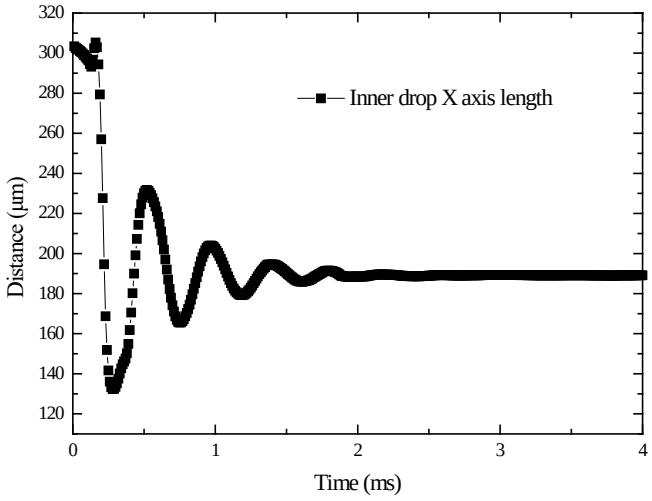

(a)

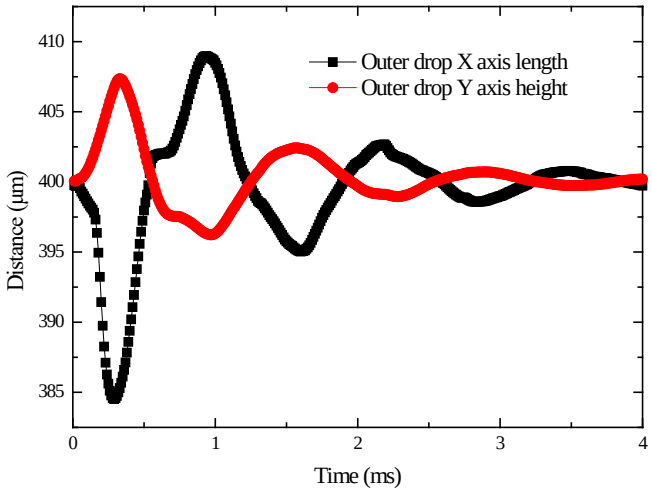

(b)

Fig. 5 (a) The distance of inner droplet along the X-axis, and (b) outer droplet along the X-axis and Y-axis.

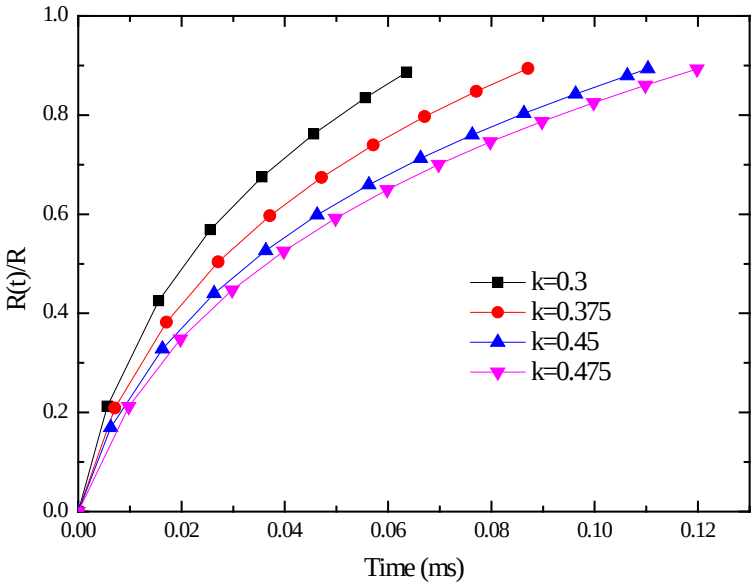

Fig. 6 The variation of the liquid bridge with time under different inner droplets' diameter.

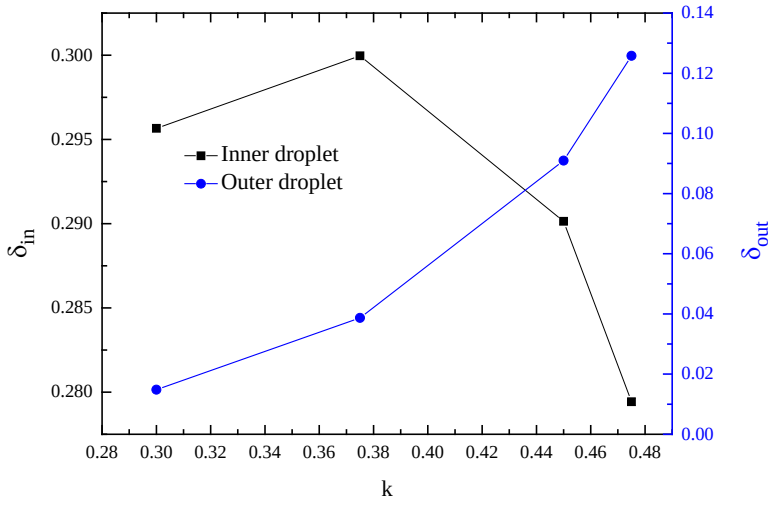

(a)

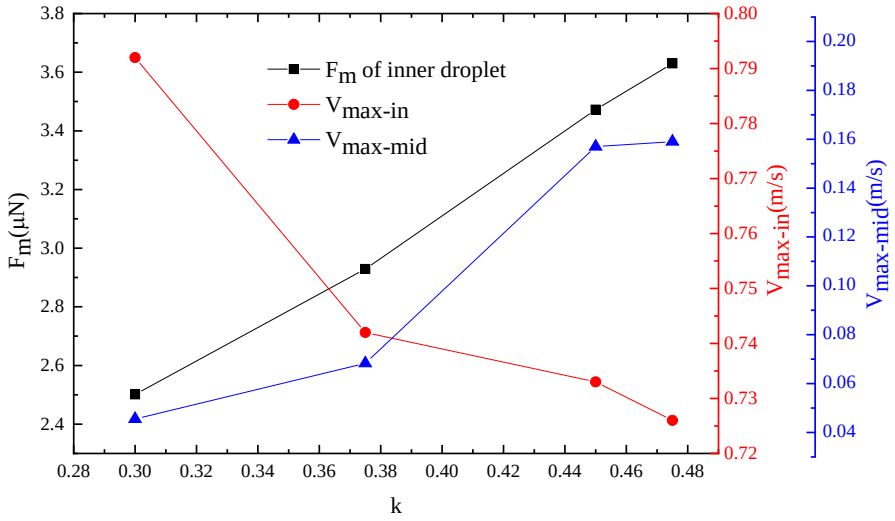

(b)

Fig. 7 (a) Effect of inner droplets' radius on the inner and outer interface deformation, and (b) the maximum velocity of the inner droplet and middle phase and the deformation resistance force of inner droplet.

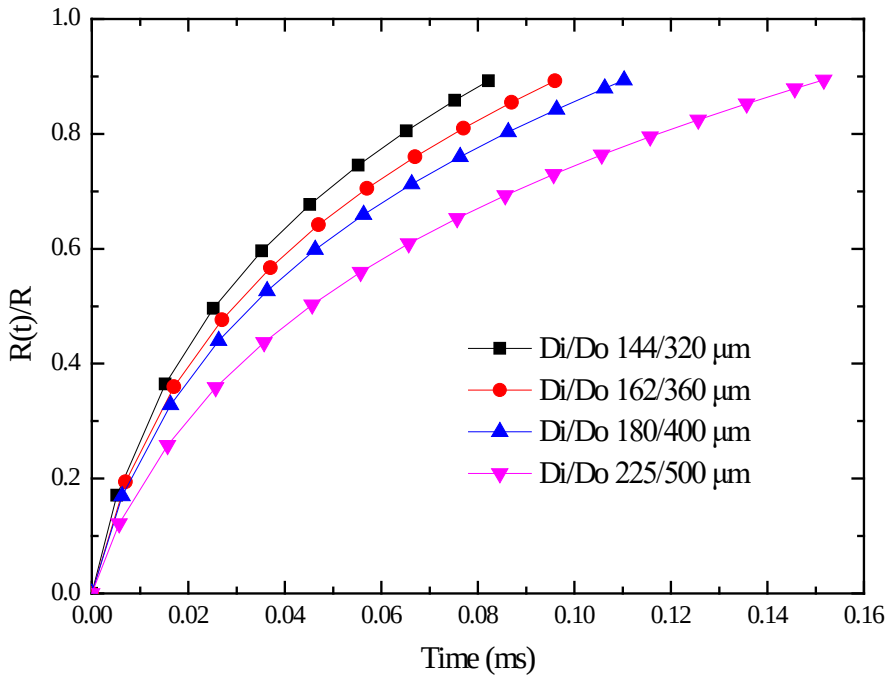

Fig. 8 Effect of the double-emulsion droplet's diameters with fixed inner-outer diameter ratio on a liquid bridge

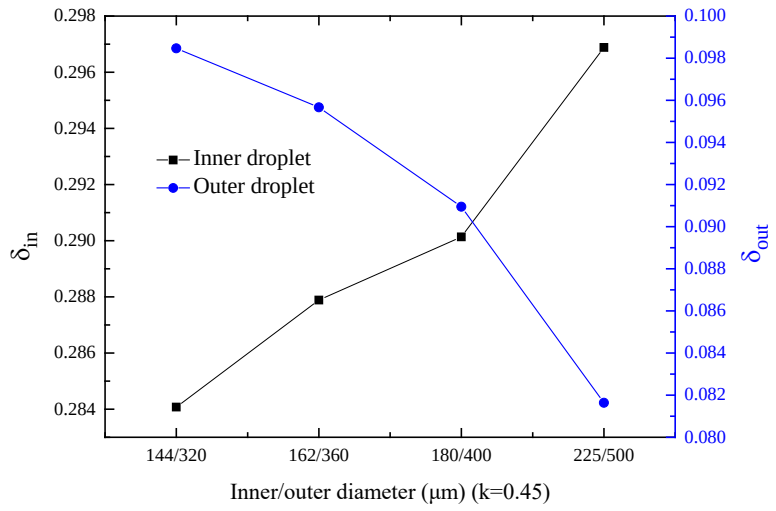

(a)

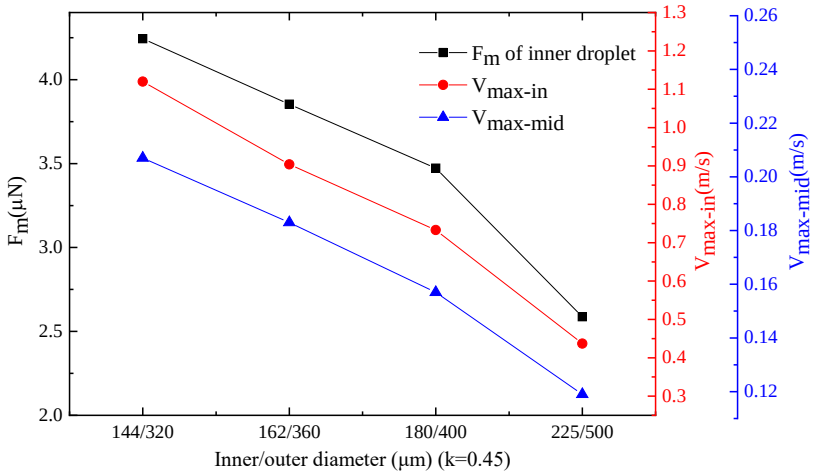

(b)

Fig. 9 (a) Effect of the double-emulsion droplet's diameters with fixed inner-outer diameter ratio on the inner and outer interface deformation, and (b) the maximum velocity of the inner droplet and middle phase and the deformation resistance force of inner droplet.

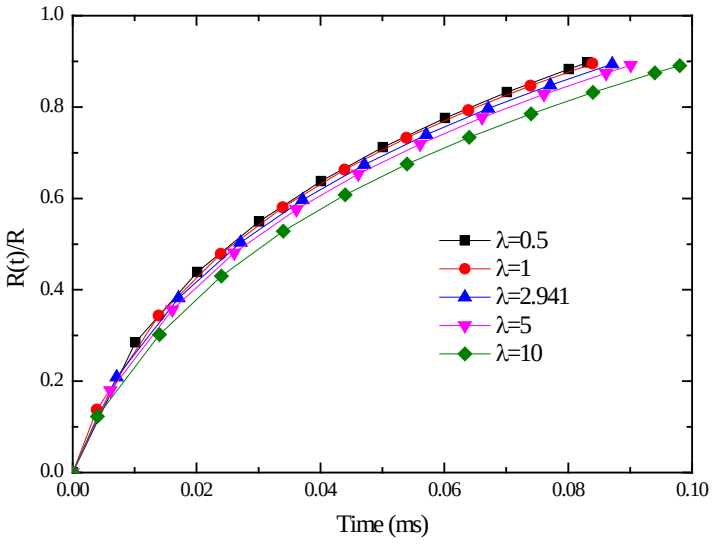

Fig. 10 The change of the liquid bridge with time under different oil viscosity.

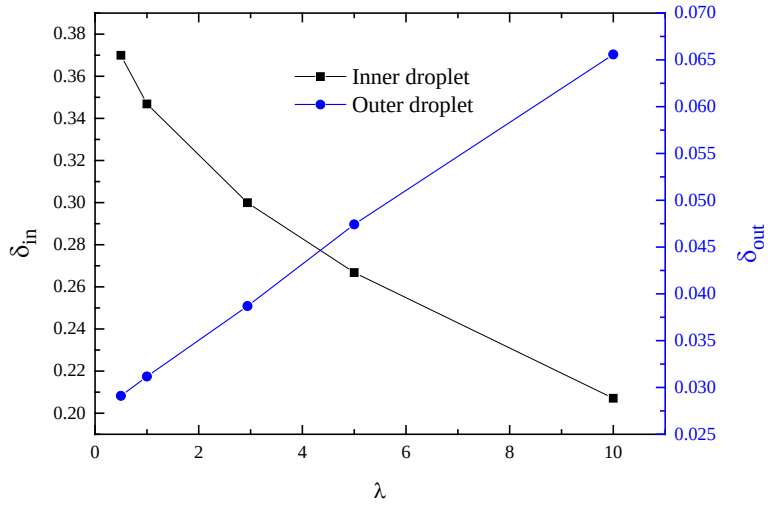

(a)

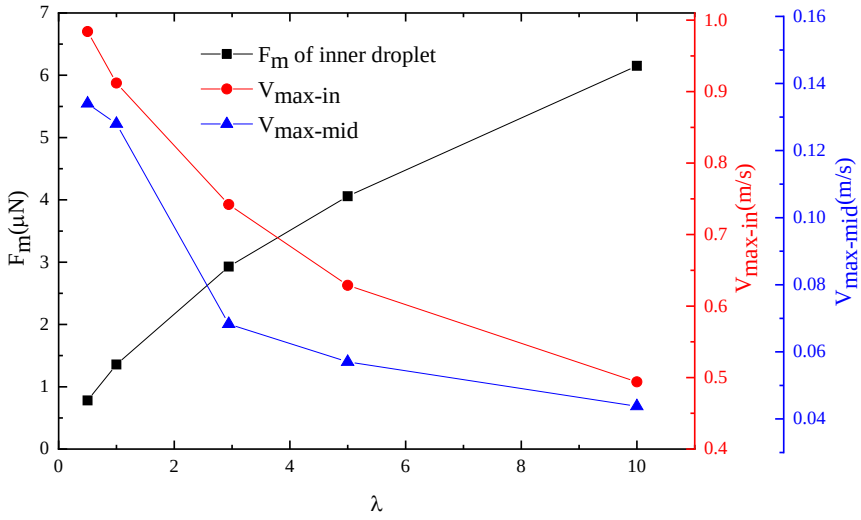

(b)

Fig. 11 (a) Effect of the oil viscosity on the inner and outer interface deformation, and (b) the maximum velocity of the inner droplet and middle phase and the deformation resistance force of inner droplet.

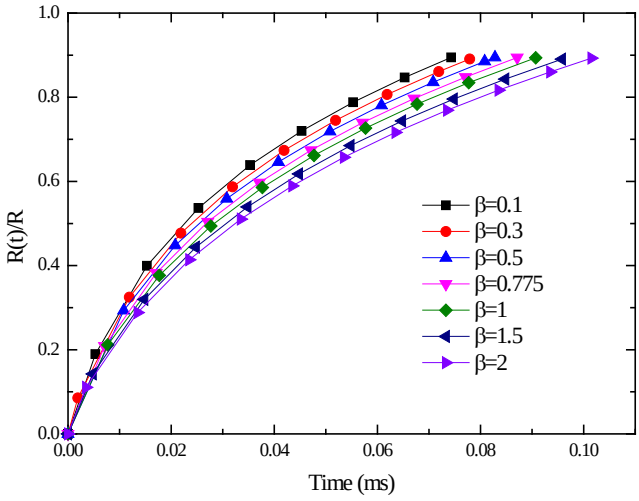

Fig. 12 The change of the liquid bridge with time under different oil density.

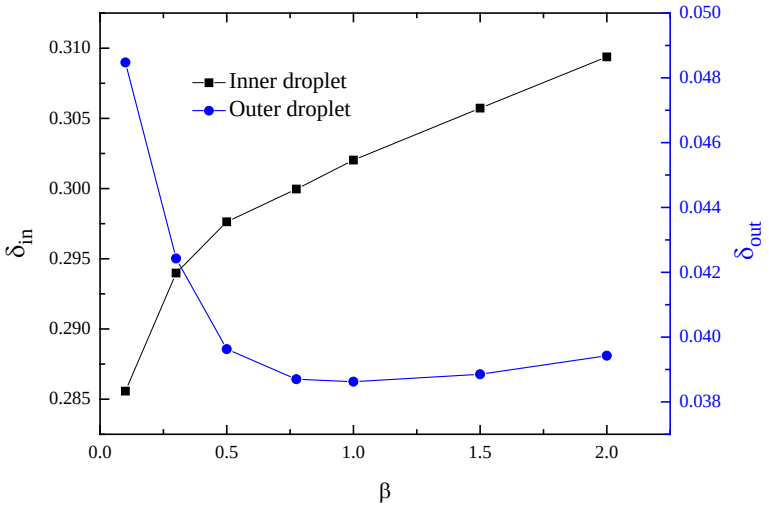

(a)

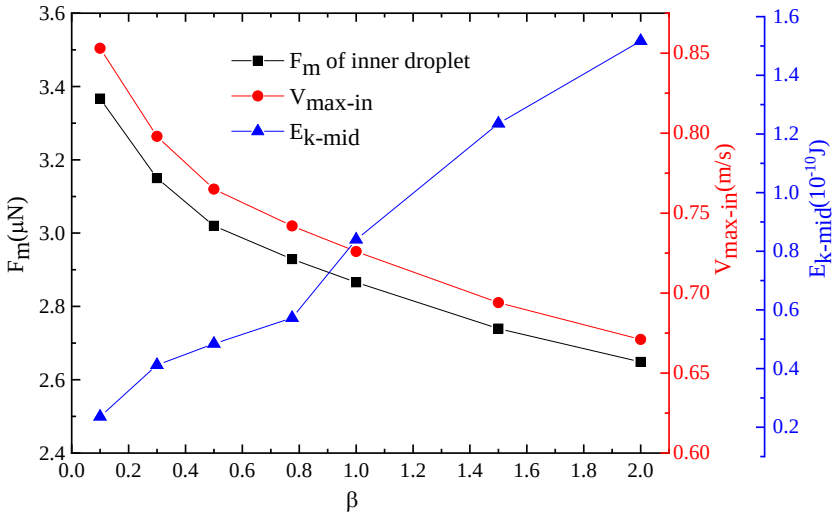

(b)

Fig. 13 (a) Effect of the oil density on the inner and outer interface deformation, and (b) the maximum velocity of the inner droplet and kinetic energy of the middle phase and the deformation resistance force of inner droplet.

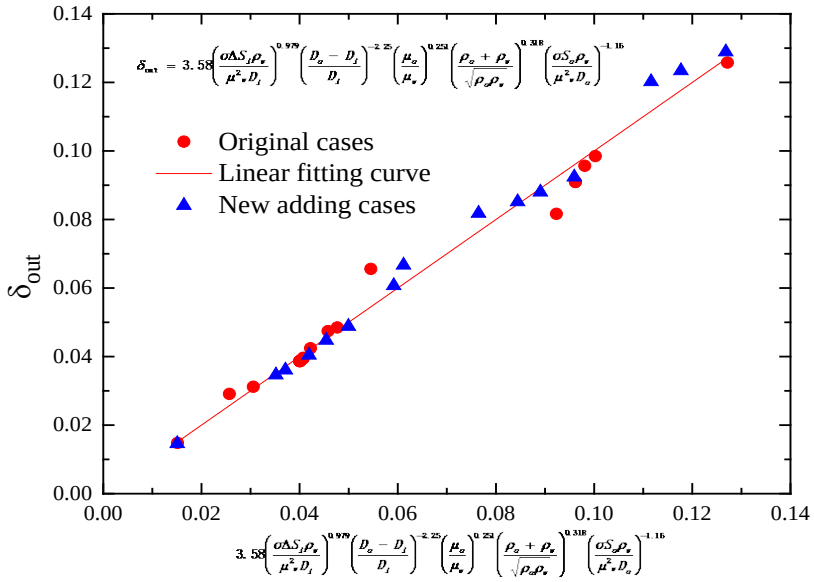

Fig. 14 The relationship between different factors and the deformation amount of outer interface.

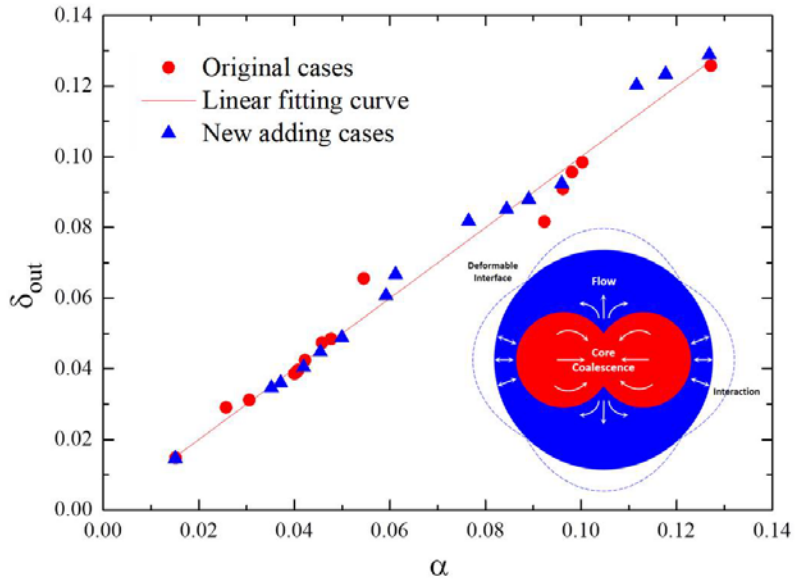

Abstract Figure

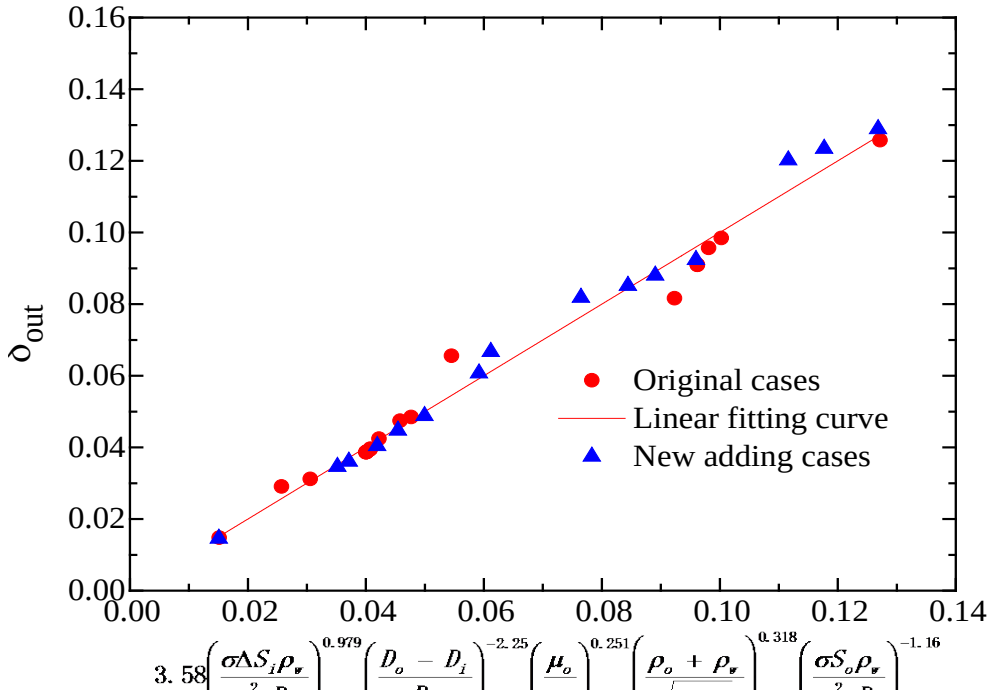
0.16
0.14
0.12
0.10
0.08
0.06
0.04
0.02
0.00
δout
0.00
0.02
0.04
0.06
0.08
0.10
0.12
0.14
Original cases
Linear fitting curve
New adding cases
3. 58